

Aggregation Schemes for Single-Vector WSI Representation Learning in Digital Pathology

Sobhan Hemati, Ghazal Alabtah, Saghir Alfasly, H.R. Tizhoosh

KIMIA Lab, Department of Artificial Intelligence and Informatics, Mayo Clinic, Rochester, MN, USA

Abstract—A crucial step to efficiently integrate Whole Slide Images (WSIs) in computational pathology is assigning a single high-quality feature vector, i.e., one embedding, to each WSI. With the existence of many pre-trained deep neural networks and the emergence of foundation models, extracting embeddings for sub-images (i.e., tiles or patches) is straightforward. However, for WSIs, given their high resolution and gigapixel nature, inputting them into existing GPUs as a single image is not feasible. As a result, WSIs are usually split into many patches. Feeding each patch to a pre-trained model, each WSI can then be represented by a set of patches, hence, a set of embeddings. Hence, in such a setup, WSI representation learning reduces to set representation learning where for each WSI we have access to a set of patch embeddings. To obtain a single embedding from a set of patch embeddings for each WSI, multiple set-based learning schemes have been proposed in the literature. In this paper, we evaluate the WSI search performance of multiple recently developed aggregation techniques (mainly set representation learning techniques) including simple average or max pooling operations, Deep Sets, Memory networks, Focal attention, Gaussian Mixture Model (GMM) Fisher Vector, and deep sparse and binary Fisher Vector on four different primary sites including bladder, breast, kidney, and Colon from TCGA. Further, we benchmark the search performance of these methods against the median of minimum distances of patch embeddings, a non-aggregating approach used for WSI retrieval.

Index Terms—Histopathology, Whole Slide Image, WSI, Image Representation, WSI Search, Set Representation Learning, Single-Vector, Aggregation.

I. INTRODUCTION

The image analysis field has witnessed remarkable advancements in recent years, thanks to the integration of deep learning models and the availability of large-scale data. However, analysis of histopathology images using deep learning is not as straightforward as ordinary-sized images. Especially, to build whole slide image (WSI) search engines, the most critical step is to be able to measure the similarity between WSIs efficiently and accurately [Tizhoosh and Pantanowitz, 2024], [Lahr et al., 2024]. The state-of-the-art approach to this step is to extract high-quality deep embeddings that capture tissue morphology from each WSI using a well-trained deep model. To this end, it is necessary to feed WSIs to build such models. However, given the gigapixel nature of WSIs, feeding a WSI at high magnification into a model to GPU memory is infeasible. To overcome this challenge, a WSI is usually split into a set of much smaller sub-images called “patches” or tiles. Following this procedure, we end up with a set of deep embeddings per WSI which makes it challenging to employ them for downstream tasks like WSI retrieval (a set

of patches that could be very large if a smart patch selection is not available). In this situation, having one single-vector WSI embedding can mitigate such challenges. With single-vector WSI representation much less memory is required to build a WSI search system. As well, using distance measures calculating similarity between WSIs becomes trivial. Finally, the search speed will increase and storage requirements will decrease resulting in wider deployment of WSI image classification and retrieval.

A practical and established approach to calculate the similarity between two sets of embeddings is the *median-of-minimums*, a scheme that was introduced as part of the Yottixel search engine [Kalra et al., 2020b]; one calculates the minimum distance of any given input patch to all other patches (of the other WSI) and takes the median of all minimum distances overall (see Fig. 1). This approach is quite practical and fast (as Yottixel used binary feature vectors) but it is not able to provide a single vector to represent WSI. A more desirable solution would be to obtain *one single embedding* per WSI for more efficient storage and more targeted WSI-to-WSI matching, or for WSI classification (Fig. 2).

To this end, different aggregation algorithms to derive a single vector of deep features from a set of patch embeddings have been proposed including simple average or max pooling operations, Deep Sets [Zaheer et al., 2017], memory networks [Kalra et al., 2020a], focal attention [Kalra et al., 2021], graph convolution neural networks [Adnan et al., 2020], Gaussian mixture model (GMM) Fisher Vector [Jaakkola and Haussler, 1999], [Perronnin and Dance, 2007], [Hemati et al., 2023], and Deep Fisher Vector and its variations (binary and sparse Fisher Vector) [Hemati et al., 2023].

Although multiple set representation learning techniques have been proposed and investigated in the literature, to the best of our knowledge, there is no study that evaluates these algorithms against each other for WSI retrieval as a challenging task. To address this shortcoming, in this paper, we briefly introduce each set representation learning technique and discuss our benchmarking scheme. Subsequently, we evaluate each method over four different datasets namely bladder, breast, kidney, and colon through the k -Nearest Neighbour (k -NN) search using WSI embeddings obtained from each method. Finally, in the result section we present and discuss the performance of each technique to generate a single vector of deep features for a WSI.

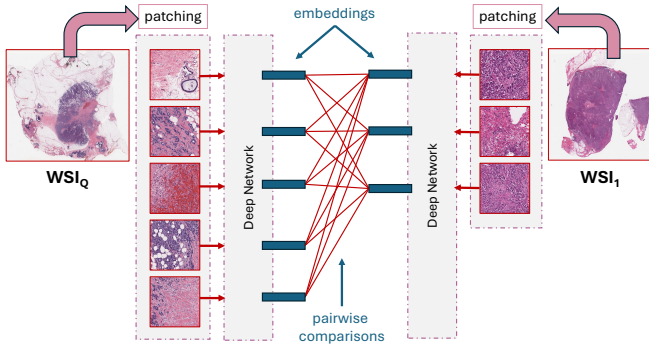


Fig. 1: Yottixel [Kalra et al., 2020b], although a patch-oriented search engine, introduced the first practical approach for WSI-to-WSI comparison through the median-of-minimum distance measurements.

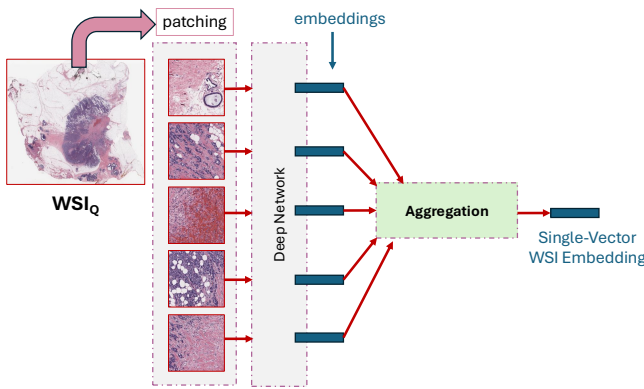


Fig. 2: Aggregation of patch embeddings can provide a single-vector WSI representation.

II. BACKGROUND

In this section, we briefly review set representation learning algorithms applied to the WSI representation learning problem.

A. GMM Fisher Vector (1999-2007)

Fisher Vector can be seen as an extension to bag of visual words (BoVW) [Csurka et al., 2004] that was initially developed in computer vision research for encoding a set of local image descriptors into one embedding. Theoretically, Fisher Vector can be developed on top of any generative models [Jaakkola and Haussler, 1999]. Some works [Perronnin and Dance, 2007] have introduced Gaussian mixture model (GMM)-based Fisher Vector which can be calculated using the gradient of the log-likelihood of the GMMs with respect to its parameters given a bag of data points (e.g., means, variances, and mixing coefficients). Theoretically, while BoVW only employs mean statistics to obtain the set representation, in the GMM-based Fisher Vector, the variance as a higher-order statistic is also used.

B. Deep Sets (2017-2021)

The Deep Set approach [Zaheer et al., 2017] focuses on permutation invariant representation learning and establish a

standard definition of the permutation invariant functions. This approach shows such a family of functions can be implemented as neural networks to learn permutation invariant representations. Other works employ Deep Sets-like architecture along with CNN to learn end-to-end WSI representations in WSI search tasks [Hemati et al., 2021]. These methods showed the obtained representations achieve better search performance both in terms of search speed and accuracy compared with Yottixel search engine [Kalra et al., 2020b].

C. Memory Networks (2020)

Other works have presented Memory-based Exchangeable Model (MEM) to learn the set functions [Kalra et al., 2020a]. MEM employs memory units and self-attention mechanisms to capture inter-dependencies between instances by mapping the input sets to high-level features. MEM was evaluated on point cloud and lung WSIs classification.

D. Focal Attention (2021)

Another set representation scheme developed for WSI classification/search is Focal attention [Kalra et al., 2021]. This approach was inspired by two recent developments in representation learning literature, namely focal loss and attention mechanism. More precisely, the focal attention approach maps single embeddings for all patches of a mosaic into a single embedding using an attention-weighted averaging modulated by a trainable focal factor.

E. Deep Fisher Vector and its variations (2023)

Motivated by the success of GMM-based Fisher Vector, Fisher Vector theory has been proposed for more recent deep generative models including Variational Autoencoders (VAEs) [Qiu et al., 2017] and GANs [Zhai et al., 2019]. Recently, other works have extended VAE-based Fisher Vectors for the WSI representation learning task [Hemati et al., 2023]. More specifically, this approach offered two variations of Deep Fisher Vectors, namely “*deep sparse Fisher Vector*” and “*deep binary Fisher Vector*”, to obtain binary and sparse permutation-invariant WSI embeddings suitable for downstream tasks such as efficient WSI search. To obtain the deep sparse and binary Fisher Vectors, one can employ a simple VAE where its latent space is also connected to a dense layer with a softmax activation function that outputs a probability distribution representing the predicted WSI class. This classifier injects class information (i.e., diagnosis) into the final WSI embeddings. Considering that the Fisher Vector is derived from the gradient space of the VAE, to achieve sparse or binary embeddings, it is desired to have sparse or minimum quantization loss gradients. This step has been performed with a gradient regularization loss which is calculated using double backpropagation [Hemati et al., 2023]. Finally, the total loss for training the VAE consists of a weighted summation of reconstruction loss, KL divergence loss, classification loss, and gradient regularization loss. The contribution of gradient regularization loss to the total loss is controlled through the α regularization parameter. Fig. 3 shows the training architecture.

After training the VAE, first, the gradients of the reconstruction loss are computed. Second, the gradient using power and L_2 normalization steps are normalized (see [Perronnin et al., 2010]). Finally, considering that the dimensionality of the deep Fisher Vector is the same as the number of the VAE parameters (which can be a large number making the WSI search expensive), the effective dimensions are selected to be the top M parameters that provide the highest variance in their respective gradient values for the training data. Fig. 4 shows the calculation of single-vector WSI representation given the trained VAE and patch embeddings for a WSI.

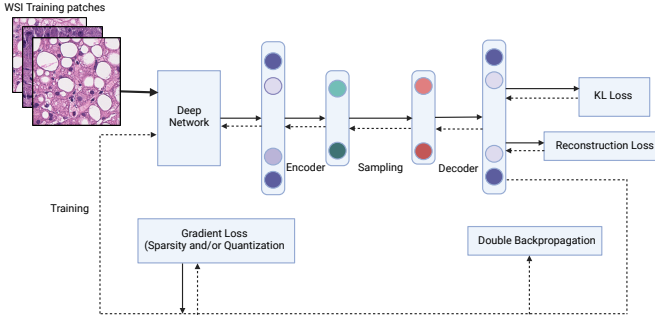


Fig. 3: VAE Training architecture

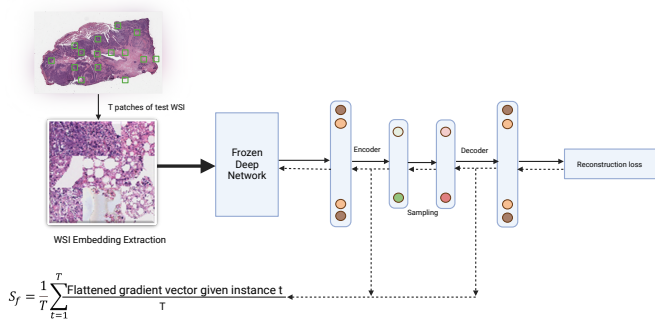


Fig. 4: Aggregation to generate a single-vector WSI embedding.

III. METHODOLOGY

This paper aims to compare the performance of the multiple set aggregation techniques for WSI representation learning including simple average or max pooling operations, Deep Sets, Memory networks, Focal attention, Gaussian Mixture Model (GMM) Fisher Vector, and deep sparse and binary Fisher Vector. We validate these methods for the task of WSI retrieval. Hence, we must construct an evaluation framework involving different datasets, and baselines. In this section, first, we discuss the datasets, the benchmarking task and baselines.

A. Datasets

The datasets presented in this study contain a collection of four histopathology cases, including bladder, breast, kidney, and colon primary sites disease cases. All datasets are drawn from The Cancer Genome Atlas (TCGA). For each

WSI, multiple patches were extracted using Yottixel’s mosaic algorithm (a two-staged clustering approach that employs stain histograms and patch proximity to group patches) [Kalra et al., 2020b]. Each patch is represented by an embedding extracted from DenseNet [Huang et al., 2017] with ImageNet pre-trained weights encoding the structural information and unique characteristics of the corresponding histological region. Patch embeddings enable quantitative analysis, facilitating comparisons among different WSI regions providing a valuable resource for exploring morphology matching, developing image analysis algorithms, and advancing diagnostic and prognostic research in oncology.

Bladder Dataset – The skin data contains 457 cases with 6 different subtypes as classes. The subtypes include ‘Transitional cell carcinoma’, ‘Papillary transitional cell carcinoma’, ‘Cholangiocarcinoma’, ‘Squamous cell carcinoma-NOS’, ‘Papillary adenocarcinoma-NOS’, ‘Carcinoma-NOS’.

Breast Dataset – The breast dataset contains 1,133 WSIs, with 23 subtypes including ‘Lobular carcinoma-NOS’, ‘Infiltrating duct carcinoma-NOS’, ‘Infiltrating duct mixed with other types of carcinoma’, ‘Adenoid cystic carcinoma’, ‘Infiltrating duct and lobular carcinoma’, ‘Intraductal micropapillary carcinoma’, ‘Large cell neuroendocrine carcinoma’, ‘Apocrine adenocarcinoma’, ‘Mucinous adenocarcinoma’, ‘Metaplastic carcinoma-NOS’, ‘Infiltrating lobular mixed with other types of carcinoma’, ‘Carcinoma-NOS’, ‘Paget disease and infiltrating duct carcinoma of breast’, ‘Pleomorphic carcinoma’, ‘Papillary carcinoma-NOS’, ‘Phyllodes tumor-malignant’, ‘Secretory carcinoma of breast’, ‘Intraductal papillary adenocarcinoma with invasion’, ‘Cribriform carcinoma-NOS’, ‘Medullary carcinoma-NOS’, ‘Tubular adenocarcinoma’, ‘Basal cell carcinoma-NOS’, ‘Malignant lymphoma-large B-cell-diffuse-NOS’.

Kidney Dataset – the kidney contains 6 subtypes and 940 cases from TCGA. The subtypes include ‘Papillary adenocarcinoma-NOS’, ‘Clear cell adenocarcinoma-NOS’, ‘Renal cell carcinoma-NOS’, ‘Giant cell sarcoma’, ‘Renal cell carcinoma-chromophobe type’, ‘Synovial sarcoma-spindle cell’.

Colon Dataset – The colon dataset has 459 cases from TCGA that contain 9 classes, ‘Adenocarcinoma-NOS’, ‘Mucinous adenocarcinoma’, ‘Adenosquamous carcinoma’, ‘Adenocarcinoma with neuroendocrine differentiation’, ‘Adenocarcinoma with mixed subtypes’, ‘Carcinoma-NOS’, ‘Papillary adenocarcinoma-NOS’, ‘Dedifferentiated liposarcoma’, ‘Malignant lymphoma-large B-cell-diffuse-NOS’.

B. Benchmarking Scheme and Baselines

WSI search and retrieval offers many benefits including teleconsultation, reduced workload, improved diagnostic quality, and expedited adoption and democratization of digital pathology through more efficient indexing of tissue images [Tizhoosh and Pantanowitz, 2018], [Janowczyk and Madabhushi, 2016], [Lahr et al., 2024], [Tizhoosh and Pantanowitz, 2024]. Considering these benefits, we are motivated to investigate the quality of WSI embeddings through the lens of k -Nearest Neighbors (k -NN) WSI search and retrieval.

Experiment	Accuracy	Macro $\bar{F}1$	Weighted $\bar{F}1$
Average Pooling	0.820	0.448	0.789
Deep Binary Fisher Vector	0.852	0.471	0.827
Deep Sets (Max)	0.835	0.473	0.804
Deep Sets (Mean)	0.846	0.513	0.828
Deep Sets (Prod)	0.824	0.470	0.799
Deep Sets (Sum)	0.833	0.427	0.797
Deep Sparse Fisher Vector	0.859	0.525	0.835
Fisher Vector	0.857	0.510	0.830
Focal Attention (Max)	0.818	0.435	0.786
Focal Attention (Mean)	0.800	0.392	0.761
Focal Attention (Sum)	0.831	0.398	0.791
Max Pooling	0.829	0.486	0.810
Memory Network (Max)	0.818	0.413	0.803
Memory Network (Mean)	0.796	0.329	0.768
Memory Network (Prod)	0.802	0.450	0.780
Memory Network (Sum)	0.837	0.362	0.780
Yottixel Median of Minima	0.796	0.375	0.757

TABLE I: Bladder Metrics

Experiment	Accuracy	Macro $\bar{F}1$	Weighted $\bar{F}1$
Average Pooling	0.667	0.103	0.615
Deep Binary Fisher Vector	0.695	0.125	0.644
Deep Sets (Max)	0.640	0.111	0.613
Deep Sets (Mean)	0.626	0.095	0.604
Deep Sets (Prod)	0.644	0.109	0.611
Deep Sets (Sum)	0.636	0.111	0.613
Deep Sparse Fisher Vector	0.692	0.132	0.647
Fisher Vector	0.692	0.146	0.639
Focal Attention (Max)	0.652	0.086	0.605
Focal Attention (Mean)	0.647	0.085	0.599
Focal Attention (Sum)	0.629	0.073	0.578
Max Pooling	0.640	0.100	0.601
Memory Network (Max)	0.588	0.068	0.545
Memory Network (Mean)	0.622	0.068	0.556
Memory Network (Prod)	0.621	0.067	0.526
Memory Network (Sum)	0.592	0.061	0.472
Yottixel Median of Minima	0.620	0.068	0.564

TABLE II: Breast Metrics

The accuracy, Macro F1 score, and weighted F1 score performance measures are used as the evaluation metrics. We benchmark multiple techniques against Yottixel’s “median of minimums” as a non-aggregation approach [Kalra et al., 2020b]. We test max and mean poolings, Gaussian Mixture Model-based Fisher Vector [Sánchez et al., 2013], Deep Sets [Zaheer et al., 2017], memory networks [Kalra et al., 2020a], focal attention [Kalra et al., 2021], and deep sparse Fisher Vector and deep binary Fisher Vector by [Hemati et al., 2023].

Except for the median of minimums, all methods lead to a single embedding per WSI. Further, the deep Fisher Vector provides both binary and sparse WSI embeddings which are ideal for fast and efficient WSI search. These representations are memory-efficient, ensuring that the embeddings can be economically stored and efficiently processed for subsequent retrieval and analysis tasks. To ensure the reliability of the results, a rigorous 5-fold cross-validation approach is employed. We compute the average and standard deviation from the five splits and use these as performance indicators.

IV. RESULTS

Tables I, II, III and IV show the evaluation results for bladder, breast, kidney, and colon datasets where *DenseNet*

was used as feature extractors. Clearly, in most cases, Deep Fisher Vector and its variations (sparse and binary) achieve the best overall performance compared with all other baselines. Here we should emphasize sparse embeddings can reduce the memory required to store embeddings while binary WSI embeddings provide both memory efficiency and extremely fast search speed by employing Hamming distance. As a sample case, we also measured the time required to conduct the colon dataset search experiment for both Deep Sparse and Binary Fisher Vectors and also the median of minimums. For the Sparse Fisher Vector, Euclidean distance is used while for the Binary Fisher Vector Hamming distance is employed. The results for this experiment are presented in Table V. Clearly, the Deep Binary Fisher Vector achieves the fastest search speed. Given that for the Sparse Fisher Vector the Euclidean distance is used, its search speed is the same as other methods that output one real-valued embedding (with the same dimension) per WSI.

A. Ablation study

To study the effect of the gradient sparsity and quantization losses for Deep Sparse and Binary Fisher vector embeddings respectively, we performed an ablation study on α for skin and lung datasets. To this end, we train the VAE for different values

Experiment	Accuracy	Macro $\bar{F}1$	Weighted $\bar{F}1$
Average Pooling	0.702	0.469	0.681
Deep Binary Fisher Vector	0.802	0.590	0.798
Deep Sets (Max)	0.763	0.549	0.756
Deep Sets (Mean)	0.760	0.549	0.755
Deep Sets (Prod)	0.747	0.535	0.741
Deep Sets (Sum)	0.764	0.547	0.756
Deep Sparse Fisher Vector	0.793	0.586	0.787
Fisher Vector	0.799	0.572	0.788
Focal Attention (Max)	0.534	0.301	0.503
Focal Attention (Mean)	0.568	0.351	0.544
Focal Attention (Sum)	0.555	0.315	0.525
Max Pooling	0.690	0.464	0.669
Memory Network (Max)	0.644	0.364	0.589
Memory Network (Mean)	0.650	0.393	0.628
Memory Network (Prod)	0.639	0.377	0.596
Memory Network (Sum)	0.492	0.163	0.331
Yottixel Median of Minima	0.472	0.248	0.441

TABLE III: Kidneys Metrics

Experiment	Accuracy	Macro $\bar{F}1$	Weighted $\bar{F}1$
Average Pooling	0.807	0.322	0.771
Deep Binary Fisher Vector	0.809	0.302	0.789
Deep Sets (Max)	0.839	0.377	0.795
Deep Sets (Mean)	0.802	0.317	0.779
Deep Sets (Prod)	0.830	0.343	0.785
Deep Sets (Sum)	0.818	0.297	0.782
Deep Sparse Fisher Vector	0.807	0.281	0.776
Fisher Vector	0.825	0.313	0.788
Focal Attention (Max)	0.807	0.332	0.770
Focal Attention (Mean)	0.816	0.322	0.769
Focal Attention (Sum)	0.825	0.327	0.776
Max Pooling	0.825	0.312	0.784
Memory Network (Max)	0.805	0.285	0.758
Memory Network (Mean)	0.798	0.301	0.754
Memory Network (Prod)	0.820	0.291	0.760
Memory Network (Sum)	0.843	0.297	0.773
Yottixel Median of Minima	0.802	0.298	0.757

TABLE IV: Colon Metrics

Dimensions	Sparse	Binary	Yottixel
30,000	1,659,800 ms	690,026 ms	1,007,515 ms
3,000	1,491,833 ms	601,359 ms	
300	1,815,617 ms	475,188 ms	

TABLE V: Time required for different dimensions of Fisher vector for Sparse and Binary methods for the Colon dataset compared to Yottixel

of α , while keeping all other hyperparameters the same. The results for breast and colon datasets are presented in Tables VI and VII. Clearly, including the regularization loss further improves the quality of embeddings while increasing memory and speed efficiency by introducing binary nature and sparsity characteristics for WSI embedding.

V. CONCLUSION

In this paper, we evaluated multiple WSI representation learning techniques including simple average or max pooling operations, deep sets, memory networks, focal attention, Gaussian Mixture Model (GMM) Fisher Vector, and deep sparse and binary Fisher Vector embeddings in the WSI search task for different datasets and two different deep models. Our evaluations show that the deep sparse and binary Fisher Vector may achieve the best overall performance compared

with multiple set aggregation schemes. This result suggests that the Fisher Vector method has a robust ability to capture relevant patterns and features within the data, regardless of the specific characteristics of each dataset. This is an important indication of the versatility and generalizability of the Fisher Vector approach. Apart from their superior WSI search performance, deep sparse and binary Fisher Vectors also offer additional advantages that are suitable for fast and efficient search and retrieval. More precisely, the sparsity in deep sparse Fisher Vector embeddings makes them occupy less storage for indexing WSIs, a crucial factor for the wide adoption and also democratization of digital pathology. Also, the deep binary Fisher Vector is significantly faster than any real-valued counterpart as the calculation of Hamming distance between binary embeddings can be calculated using the XOR gate at the CPU level which is extremely faster than Euclidean distance.

REFERENCES

- [Adnan et al., 2020] Adnan, M., Kalra, S., and Tizhoosh, H. R. (2020). Representation learning of histopathology images using graph neural networks. In *Proceedings of the IEEE/CVF Conference on Computer Vision and Pattern Recognition Workshops*, pages 988–989.
- [Csurka et al., 2004] Csurka, G., Dance, C., Fan, L., Willamowski, J., and Bray, C. (2004). Visual categorization with bags of keypoints. In *Workshop on statistical learning in computer vision, ECCV*, volume 1, pages 1–2. Prague.

α	Breast (Sparse)			Breast (Binary)		
	Accuracy	Macro $\bar{F}1$	Weighted $\bar{F}1$	Accuracy	Macro $\bar{F}1$	Weighted $\bar{F}1$
0.0	0.690	0.151	0.651	0.685	0.126	0.640
0.1	0.693	0.149	0.650	0.703	0.131	0.653
0.01	0.698	0.140	0.651	0.697	0.123	0.646
0.001	0.702	0.145	0.660	0.684	0.115	0.636
0.0001	0.688	0.137	0.646	0.691	0.114	0.637
0.00001	0.706	0.144	0.663	0.680	0.116	0.634

TABLE VI: Results for Sparse and Binary Fisher vector methods for Breast dataset with different values of α , including Accuracy, Macro $\bar{F}1$, and Weighted $\bar{F}1$

α	Colon (Sparse)			Colon (Binary)		
	Accuracy	Macro $\bar{F}1$	Weighted $\bar{F}1$	Accuracy	Macro $\bar{F}1$	Weighted $\bar{F}1$
0.0	0.825	0.358	0.789	0.807	0.274	0.778
0.1	0.820	0.339	0.782	0.807	0.307	0.785
0.01	0.820	0.340	0.782	0.811	0.277	0.783
0.001	0.814	0.330	0.776	0.818	0.288	0.790
0.0001	0.816	0.316	0.778	0.820	0.312	0.786
0.00001	0.816	0.334	0.780	0.805	0.301	0.779

TABLE VII: Results for Sparse and Binary Fisher vector methods for Colon dataset with different values of α , including Accuracy, Macro $\bar{F}1$, and Weighted $\bar{F}1$

- [Hemati et al., 2023] Hemati, S., Kalra, S., Babaie, M., and Tizhoosh, H. (2023). Learning binary and sparse permutation-invariant representations for fast and memory efficient whole slide image search. *Computers in Biology and Medicine*, 162:107026.
- [Hemati et al., 2021] Hemati, S., Kalra, S., Meaney, C., Babaie, M., Ghodsi, A., and Tizhoosh, H. (2021). Cnn and deep sets for end-to-end whole slide image representation learning. In *Medical Imaging with Deep Learning*, pages 301–311. PMLR.
- [Huang et al., 2017] Huang, G., Liu, Z., Van Der Maaten, L., and Weinberger, K. Q. (2017). Densely connected convolutional networks. In *Proceedings of the IEEE conference on computer vision and pattern recognition*, pages 4700–4708.
- [Jaakkola and Haussler, 1999] Jaakkola, T. and Haussler, D. (1999). Exploiting generative models in discriminative classifiers. In *Advances in neural information processing systems*, pages 487–493.
- [Janowczyk and Madabhushi, 2016] Janowczyk, A. and Madabhushi, A. (2016). Deep learning for digital pathology image analysis: A comprehensive tutorial with selected use cases. *Journal of pathology informatics*, 7.
- [Kalra et al., 2021] Kalra, S., Adnan, M., Hemati, S., Dehkharghanian, T., Rahnamayan, S., and Tizhoosh, H. R. (2021). Pay attention with focus: A novel learning scheme for classification of whole slide images. In *Medical Image Computing and Computer Assisted Intervention–MICCAI 2021: 24th International Conference, Strasbourg, France, September 27–October 1, 2021, Proceedings, Part VIII 24*, pages 350–359. Springer.
- [Kalra et al., 2020a] Kalra, S., Adnan, M., Taylor, G., and Tizhoosh, H. R. (2020a). Learning permutation invariant representations using memory networks. In *Computer Vision–ECCV 2020: 16th European Conference, Glasgow, UK, August 23–28, 2020, Proceedings, Part XXIX 16*, pages 677–693. Springer.
- [Kalra et al., 2020b] Kalra, S., Tizhoosh, H. R., Choi, C., Shah, S., Diamandis, P., Campbell, C. J., and Pantanowitz, L. (2020b). Yottixel—an image search engine for large archives of histopathology whole slide images. *Medical Image Analysis*, 65:101757.
- [Lahr et al., 2024] Lahr, I., Alfasly, S., Nejat, P., Khan, J., Kottom, L., Kumbhar, V., Alsaafin, A., Shafique, A., Hemati, S., Alabtah, G., Comfere, N., Murphree, D., Mangold, A., Yasir, S., Meroueh, C., Boardman, L., Shah, V. H., Garcia, J. J., and Tizhoosh, H. (2024). Analysis and validation of image search engines in histopathology. *IEEE Reviews in Biomedical Engineering*, pages 1–19.
- [Perronnin and Dance, 2007] Perronnin, F. and Dance, C. (2007). Fisher kernels on visual vocabularies for image categorization. In *2007 IEEE conference on computer vision and pattern recognition*, pages 1–8. IEEE.
- [Perronnin et al., 2010] Perronnin, F., Sánchez, J., and Mensink, T. (2010). Improving the fisher kernel for large-scale image classification. In *Computer Vision–ECCV 2010: 11th European Conference on Computer Vision, Heraklion, Crete, Greece, September 5–11, 2010, Proceedings, Part IV 11*, pages 143–156. Springer.
- [Qiu et al., 2017] Qiu, Z., Yao, T., and Mei, T. (2017). Deep quantization: Encoding convolutional activations with deep generative model. In *Proceedings of the IEEE Conference on Computer Vision and Pattern Recognition*, pages 6759–6768.
- [Sánchez et al., 2013] Sánchez, J., Perronnin, F., Mensink, T., and Verbeek, J. (2013). Image classification with the fisher vector: Theory and practice. *International journal of computer vision*, 105(3):222–245.
- [Tizhoosh and Pantanowitz, 2018] Tizhoosh, H. R. and Pantanowitz, L. (2018). Artificial intelligence and digital pathology: challenges and opportunities. *Journal of pathology informatics*, 9.
- [Tizhoosh and Pantanowitz, 2024] Tizhoosh, H. R. and Pantanowitz, L. (2024). On image search in histopathology. *Journal of Pathology Informatics*, page 100375.
- [Zaheer et al., 2017] Zaheer, M., Kottur, S., Ravanbakhsh, S., Poczos, B., Salakhutdinov, R. R., and Smola, A. J. (2017). Deep sets. *Advances in neural information processing systems*, 30.
- [Zhai et al., 2019] Zhai, S., Talbott, W., Guestrin, C., and Susskind, J. (2019). Adversarial fisher vectors for unsupervised representation learning. *Advances in Neural Information Processing Systems*, 32.